ELSEVIER

Ceramics International 32 (2006) 249–255

CERAMICS INTERNATIONAL

www.elsevier.com/locate/ceramint

Fracture toughness of alumina–zirconia composites

F. Cesari [a,*], L. Esposito [b], F.M. Furgiuele [c,*], C. Maletta [c], A. Tucci [b]

[a] *DIEM, Engineering Faculty, University of Bologna, Viale Risorgimento 2, 40136 Bologna, Italy*
[b] *Centro Ceramico, Via Martelli 26, 40138 Bologna, Italy*
[c] *Mechanical Engineering Department, University of Calabria, Ponte P. Bucci 44C, 87030 Arcavacata di Rende, CS, Italy*

Received 27 November 2004; received in revised form 4 January 2005; accepted 8 February 2005
Available online 16 June 2005

Abstract

The toughening effect in the alumina–zirconia system was simulated by a simple model based on two concentric spheres and a crack in the matrix, near the interface of the inclusion. The effects due to the zirconia $t \rightarrow m$ phase transformation and the thermal stresses, which develop during the cooling stage of sintering, were also taken into account. The toughening effect was simulated imposing a temperature field both to the matrix and the inclusion and the analysis was carried out at different temperatures. The results of the simulation at room temperature were compared with the experimental data of fracture toughness obtained testing alumina–zirconia composites, containing different percentages of the oxides.

Keywords: Al_2O_3–ZrO_2 composites; Stress intensity factor; Fracture toughness; Zirconia $t \rightarrow m$ phase transformation

1. Introduction

The demand for even more reliable structural components by the advanced industrial sectors, encouraged the development and use of innovative materials, i.e. ceramic materials [1]. The properties of the advanced ceramics are particularly attractive for structural applications such as in the motor, aerospace and biomedical fields, especially when the environmental conditions are particularly severe. As well known, the problem of the low fracture toughness of ceramics can be overcome designing and preparing composite materials reinforced with fibres, whiskers and particles, or zirconia based ceramics [2]. As regards, for this last class of materials, the increase in fracture toughness can be attributed to different mechanisms: (i) the $t \rightarrow m$ phase transformation [3,4] (ii) crack deflection [5], and (iii) microcracking of the matrix [6]. In zirconia based ceramics the relationships between mechanical properties and microstructure are strictly influenced by the zirconia grain size, resulting in the efficiency of the phase transformation [7] and development of microcracks [8]. Very important can be also the contribution of residual stresses arising during the cooling stage of sintering. As regards, in alumina–zirconia composites the alumina particles are subjected to a compressive stress field, due to their lower thermal expansion coefficient [9,10].

The aim of the present study was to analyse the thermal–mechanical behaviour of the alumina–zirconia system. Starting from pure oxides, several composites containing different percentages of the two components were considered. Alumina, probably the best reinforcing agent for a zirconia matrix, increases the Young's modulus, prevents the anomalous growth of zirconia grains in the cubic phase and activates a toughening mechanism, interacting with the cracks during their propagation [11]. In an alumina matrix, zirconia in the tetragonal phase favours a toughening mechanism via the $t \rightarrow m$ phase transformation and induces a residual stress field due to the different thermal expansion coefficient [3].

The study reports the results regarding the possibility to predict the fracture behaviour of alumina–zirconia composites, by using a simple model in which the effects of the $t \rightarrow m$ phase transformation and the thermal stresses induced

* Corresponding authors. Tel.: +39 0984 494827; fax: +39 0984 494673.
E-mail address: furgiuele@unical.it (F.M. Furgiuele).

0272-8842/$30.00
doi:10.1016/j.ceramint.2005.02.012

during the cooling stage of sintering by the different thermal expansion coefficients of the components, were taken into account. The results were checked with experimental data of fracture toughness.

2. Model description

The analysis of the composite was performed considering a representative volume element, RVE, containing the constitutive materials. It can be useful to consider representative volume elements for idealised particle-packing geometries such as cube and tetrahedron arrays, Fig. 1. Assuming the cube array, the volume fraction v_f found by dividing the volume of inclusion enclosed into cube by the total cube volume, is:

$$v_f = \left(\frac{4}{3}\pi r_f^3\right)\frac{1}{8b^3} = \frac{\pi}{6}\left(\frac{r_f}{b}\right)^3 \quad (1)$$

where $2b$ is the inclusion spacing and r_f is the radius of the inclusion.

The RVE for the cube array in Fig. 1(a) is show in Fig. 2(a). By the conversion of the RVE to a sphere matrix having the same volume as the cube matrix, the radius r_m of the equivalent sphere in Fig. 2(b) is:

$$r_m = \left(\frac{6}{\pi}\right)^{1/3} b \quad (2)$$

Substituting the Eq. (1) in (2), the radius of the equivalent sphere becomes:

$$r_m = (v_f)^{-1/3} r_f \quad (3)$$

The model consists in a spherical inclusion r_f in radius, the inclusion, embedded in an another sphere r_m in radius, the matrix. Besides, assuming that in the matrix is present a crack contiguous to the interface and randomly orientated, the cracks interaction is actually excluded. The fracture behaviour of alumina–zirconia composites was analysed determining the stress intensity factor for different ratios r_m/r_f, when an uniform tensile loading p is applied to the matrix surface.

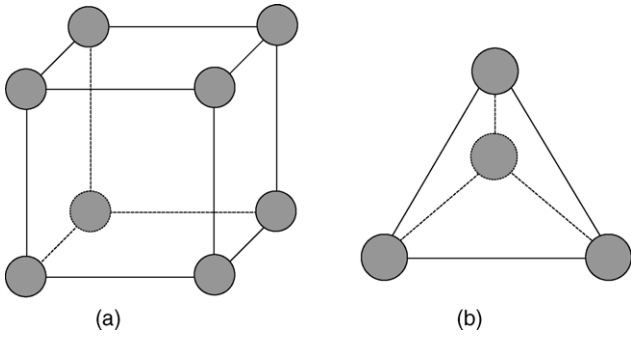

Fig. 1. Representative volume elements, RVE, for idealised particle-packing geometries: (a) cube array and (b) tetrahedron array.

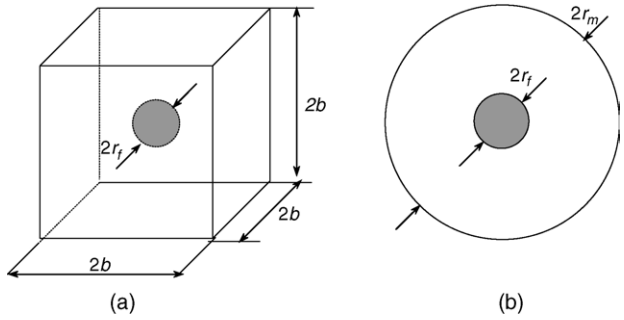

Fig. 2. (a) RVE for the cube array in Fig. 1(a) and (b) equivalent sphere matrix having the same volume the cube matrix.

The thermal stress field originated by the thermal expansion coefficient of alumina lower than that of zirconia was simulated imposing an uniform temperature field both to the matrix and the particle.

In the work only the volume increase, 3–5%, as consequence of the $t \rightarrow m$ phase transformation was taken into account, neglecting the lattice distortion, 1–7%. The volume increase was simulated by a thermal effect, imposing different temperatures to the matrix and the inclusion. Then, the analysis was carried out considering two different loading conditions: (a) the first, of mechanical source, due to the tensile load applied at the surface of the matrix, and (b) the second, of thermal source, induced by a different field temperature imposed to the matrix and particle, respectively.

The stress field induced by the mechanical loading condition both to the inclusion and the matrix was determined by the solution suggested in [11]. In particular, the solution in terms of displacements and stresses regarding the hallow sphere, the matrix, is given by the relations:

$$\begin{aligned} u_m &= C_1 r + C_2/r^2 \\ \sigma_{rm} &= \frac{E_m C_1}{1-2\nu_m} - \frac{2E_m C_2}{1+\nu_m}\frac{1}{r^3} \\ \sigma_{tm} &= \frac{E_m C_1}{1-2\nu_m} + \frac{E_m C_2}{1+\nu_m}\frac{1}{r^3} \end{aligned} \quad (4)$$

where u is the radial displacement, σ_r and σ_t are the radial and hoop stress, respectively, E and ν are the Young's modulus and the Poisson's coefficient of the material, r is a generic radius and C_1 and C_2 constants deriving from the boundary conditions.

Similarly, the solution for the solid sphere, the particle, is given by the relations:

$$\begin{aligned} u_f &= C_3 r \\ \sigma_{rf} &= \frac{E_f C_3}{1-2\nu_f} \\ \sigma_{tf} &= \frac{E_f C_3}{1-2\nu_f} \end{aligned} \quad (5)$$

where the symbols are the same of the Eq. (4) and C_3 a constant function of the boundary conditions. The constants C_1, C_2 and C_3 have been determined imposing the

following conditions:

$$\begin{aligned} u_m &= u_f \quad \text{at} \quad r = r_f \\ \sigma_{rm} &= \sigma_{rf} \quad \text{at} \quad r = r_f \\ \sigma_{rm} &= p \quad \text{at} \quad r = r_m \end{aligned} \tag{6}$$

When the matrix and the inclusion are subjected to an uniform temperature, T_m and T_f, respectively, the displacements and the stresses rising in the matrix can be expressed as:

$$\begin{aligned} u_m &= \frac{1}{3}\frac{1+\nu_m}{1-\nu_m}\alpha_m T_m \frac{r^3 - r_f^3}{r^2} + C_4 r + \frac{C_5}{r^2} \\ \sigma_{rm} &= -\frac{2\alpha_m E_m}{1-\nu_m} T_m \frac{r^3 - r_f^3}{3r^3} - \frac{E_m C_4}{1-2\nu_m} - \frac{2E_m C_5}{1+\nu_m}\frac{1}{r^3} \\ \sigma_{tm} &= \frac{\alpha_m E_m}{1-\nu_m} T_m \frac{r^3 - r_f^3}{3r^3} + \frac{E_m C_4}{1-2\nu_m} + \frac{E_m C_5}{1+\nu_m}\frac{1}{r^3} \end{aligned} \tag{7}$$

while for the inclusion:

$$\begin{aligned} u_f &= \frac{1}{3}\frac{1+\nu_f}{1-\nu_f}\alpha_f T_f r + C_6 r \\ \sigma_{rf} &= -\frac{2\alpha_f E_f}{3(1-\nu_f)} T_f - \frac{E_f C_6}{1-2\nu_f} \\ \sigma_{tf} &= \frac{\alpha_f E_f}{3(1-\nu_f)} T_f - \frac{\alpha_f E_f}{1-\nu_f} T_f + \frac{E_f C_6}{1-2\nu_f} \end{aligned} \tag{8}$$

The constants C_4, C_5 and C_6 are determined from the two first conditions of the Eq. (6), assuming $\sigma_{rm} = 0$ at $r = r_m$.

The unstable propagation of the crack starts when the stress field, function of the dimensions and the geometry of the crack and the mechanisms defining its trigger, reaches the critical value. It can be reasonable to believe that the critical conditions are reached at particular combinations of σ_n, the stress perpendicular to the plane containing the crack and τ, the maximum shear stress acting in the same plane. The two components can be expressed as a function of the principal stresses σ_1, σ_2 and σ_3, by the relations:

$$\begin{aligned} \sigma_n &= \sigma_1 l_1^2 + \sigma_2 l_2^2 + \sigma_3 l_3^2 \\ \tau &= \sqrt{\sigma_1^2 l_1^2 + \sigma_2^2 l_2^2 + \sigma_3^2 l_3^2 - \sigma_n^2} \end{aligned} \tag{9}$$

where l_1, l_2 and l_3 are the direction cosines, Fig. 3.

$$\begin{aligned} l_1 &= \sin\alpha \cos\beta \\ l_2 &= \sin\alpha \sin\beta \\ l_3 &= \cos\alpha \end{aligned}$$

Once chosen the crack geometry and the fracture criterion, to identify the combinations of σ_n and τ reaching the critical condition, it is necessary to define an equivalent stress depending on the loading condition and the orientation of the crack in respect to the principal directions:

$$\sigma_e = f[\sigma_n(\alpha, \beta),\ \tau(\alpha, \beta)]$$

In the model, σ_1 and σ_2 coincide with the hoop stress σ_{tm} while σ_3 coincides with the radial stress σ_{rm}. Under these hypotheses, apart from the fracture criterion and the crack propagation coplanar [12] or not [13] with the plane, a crack near to the interface reaches the critical condition when the direction of its axis is radial.

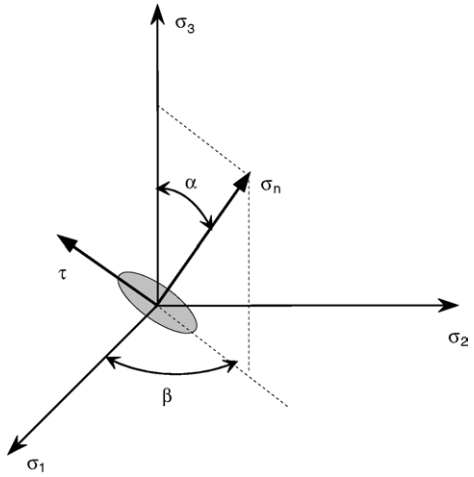

Fig. 3. Orientation of the crack with respect to the principal directions.

The stress intensity factor K_I pertinent to a crack $2a$ in length, the centre of which lies to the radius r_a, Fig. 4, can be determined by the equation [14]:

$$K_I = \frac{1}{\sqrt{\pi a}} \int_{-a}^{a} \sqrt{\frac{a+t}{a-r}}\sigma_{tm}(t)\,dt \tag{10}$$

where t is defined in Fig. 4.

Because of the particular form of the product of the two functions changing t, the integration of the Eq. (10) is not possible. However, considering the average value of the hoop stresses $\bar{\sigma}_{tm}$, the Eq. (10) becomes:

$$K_I = \bar{\sigma}_{tm}\sqrt{\pi a} \tag{11}$$

where $\bar{\sigma}_{tm}$ is defined as:

$$\bar{\sigma}_{tm} = \frac{\int_{-a}^{a} \sigma_{tm}(t)\,dt}{2a} \tag{12}$$

3. Materials and experimental

The alumina and zirconia samples were prepared using the powders SM8 (Baikowski, F) and zirconia stabilized by

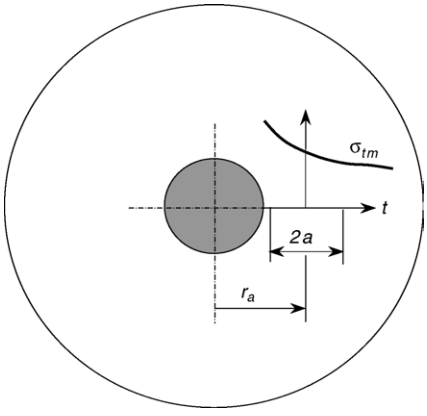

Fig. 4. Crack near the interface.

Table 1
Composition and characteristics of the selected powders

Powder	Composition (weight %)		Surface area (m^2/g)	Average particles size (μm)	
	Y-ZrO_2	Al_2O_3		ZrO_2	Al_2O_3
Z	100	0	7	0.2	–
8Z2A	80	20	16	<0.1	<0.3
6Z4A	60	40	15	<0.3	<0.3
4Z6A	40	60	12	<0.3	<0.3
2Z8A	20	80	10	<0.1	<0.3
A	0	100	10	–	0.2

3 mol% Y_2O_3 (TZ3YS—Tosoh Co., J) respectively, denoted as A and Z. The composites were prepared using the powders TZ3Y20A, TZ3Y40A, TZ3Y60A and TZ3Y80A (Tosoh Co., J) containing 20, 40, 60 and 80 wt% of alumina, respectively and denoted in the following as 8Z2A, 6Z4A, 4Z6A and 2Z8A. In Table 1 are reported the compositions and the characteristics of the powders. The samples prepared by slip casting [15], were first dried and then sintered in air at different temperatures from 1500 to 1600 °C, depending on the powder composition. The most important physical-morphological characteristics of the sintered materials are summarised in Table 2. They showed a homogeneous dispersion of the alumina and zirconia grains and reached a density 99.5–100% of the theoretical density. The grain size is generally submicronic and no anomalous growth of alumina grains was found. X-ray diffraction analyses showed that the alumina is present in the α form and the zirconia is always in the tetragonal phase.

The flexural strength of the materials was determined by four-points bending, testing specimens in form of bars, obtained by cutting the disks, with rectangular cross section 2 mm × 2.5 mm × 25 mm with a tolerance of ±0.2 mm. According to the recommendations reported in the Standard EN 843-1 [16], the longitudinal edges of the specimens were chamfered to 45° and then polished to eliminate the edge cracks induced by cutting. Besides, the surface to subject to tensile stress was polished to eliminate the cracks induced by machining. Finally, to relax the residual stresses due to machining the specimens were thermally treated at 1200 °C for 1 h. The tests were carried out by an universal machine (MTS, 10/M, USA), with a crosshead speed of 5 mm/min. The outer and the inner rollers spans were 20 and 10 mm, respectively. Table 3 reports both the bending strength σ_R

Table 2
Physical and microstructural characteristics of the sintered ceramics

Material	Density (g/cm^3)	Average grain size (μm)	
		ZrO_2	Al_2O_3
Z	6.05	0.74	–
8Z2A	5.48	0.60	0.68
6Z4A	5.02	0.36	0.29
4Z6A	4.60	0.25	0.37
2Z8A	4.27	0.25	0.60
A	3.95	–	3.40

Table 3
Mechanical characteristics of the sintered ceramics

Material	σ_R (MPa)	m	σ_θ (MPa)	E (GPa)	HV (GPa)	K_{IC} (MPa $m^{1/2}$)
Z	766	11.7	810	205	13.3	4.3
8Z2A	811	13.3	831	246	14.3	5.0
6Z4A	912	7.3	977	285	15.1	5.2
4Z6A	834	11.4	874	316	16.4	3.6
2Z8A	717	7.7	763	348	17.8	4.1
A	436	9.7	460	356	18.3	4.2

and the corresponding values of Young's modulus determined measuring the deformation of the bars by an extensometer, average of at least 20 valid results. The Weibull's parameters m and σ_θ were also determined, adopting as probability estimator $P_i = (i - 0.5)/N$.

The critical stress intensity factor K_{IC} was evaluated by Vickers indentation technique, using the Anstis formula [17]:

$$K_{IC} = 0.016 H \left(\frac{E}{H}\right)^{1/2} \left(\frac{P}{c^{3/2}}\right) \tag{13}$$

where P is the indentation-applied load, c is the length of the cracks arising from the corners of the impression and E and H are respectively the Young's modulus and Vickers hardness. In Table 3 are reported Vickers hardness and fracture toughness values, average of at least 10 valid tests carried out by a hardness tester (Zwick, 3212, D), applying as indentation loads 196.2 and 98.1 N, respectively.

4. Results and discussion

4.1. Room temperature analysis

In the present analysis the radius r_m of the sphere matrix was kept constant, while the radius r_f of the inclusion and the crack length $2a$ was changed. For each value of the inclusions percentage, the radius r_f was determined by the Eq. (3). The length of the radius r_m was kept 100 μm.

The Poisson's coefficient of alumina and zirconia was assumed equal to 0.32. The linear thermal expansion coefficients for the two materials are [18]:

$$\begin{aligned} \alpha_A &= (6.6)10^{-6} + (4.1)10^{-9}T - (8.9)10^{-13}T^2 \\ \alpha_Z &= (9.75)10^{-6} + (4.0)10^{-9}T - (1.44)10^{-12}T^2 \end{aligned} \tag{14}$$

where T is the temperature expressed in (K) and the subscripts A and Z refer to alumina and zirconia, respectively. The equations are valid in the range of temperature from 25 to 1500 °C.

The analyses were performed for two phases. In the first, the matrix was considered to be alumina the inclusions zirconia and the corresponding composite denoted as Material 1. The second was just the opposite, the matrix was considered to be zirconia the inclusions alumina and denoted as Material 2. In both cases the centre of the crack,

Table 4
Material 1: dimensionless stress intensity factor K_I/K_0 for different volume percentages of ZrO_2 and crack length $2a$

Inclusion ZrO_2 (%)	K_I/K_0		
	$a = r_m/100$	$a = r_m/50$	$a = r_m/25$
5	1.111	1.107	1.100
10	1.123	1.120	1.114
15	1.135	1.133	1.127
20	1.148	1.145	1.140
25	1.161	1.158	1.154
30	1.174	1.171	1.167
35	1.187	1.184	1.180
40	1.200	1.198	1.194
45	1.214	1.212	1.208

$2a$ in length, was considered far $1.01a$ from the interface or at a radius $r_a = (r_f + 1.01a)$. The analyses were carried out for three different values of the crack length $2a$ ($r_m/100$, $r_m/50$, and $r_m/25$) and nine different percentages referred to the total volume of inclusions, in the range 5–45%.

The K_I values for Material 1 normalised to K_0, are reported in Table 4, where $K_0 = \sigma\sqrt{\pi a}$ represents the stress intensity factor of the pure material subjected to a tensile stress p applied to the outside edge. The values show an increase of K_I with the increase of the inclusions percentage and a decrease with the increase of the crack length. This last condition takes place when the effect due to the average stress prevails over the crack length. In any case, with the increase of the inclusions percentage, the differences decrease from 0.6 to 0.3%. The behaviour of the ratio K_I/K_0, as a function of the volume percentage of zirconia, is reported in Fig. 5. The results are referred to a crack length $2a = r_m/50$, while the upper and the lower shifts are relative to $2a = r_m/100$ and $2a = r_m/25$, respectively.

The thermal stress field due to the thermal expansion coefficient of the alumina lower than that of zirconia and simulated by imposing a field temperature T, both to the matrix and the inclusion, determines an increase of K_I, see Fig. 5. In these conditions, the matrix is subjected to a radial compressive stress that causes an increase of the hoop stress and, consequently, of K_I. The increases of K_I due to a set up temperature of 25 °C are included in the 1% and for the highest inclusions percentage, it results not much higher. Also in this case, changing the crack length, the differences among the K_I values are similar to those of the previous analysis. As regards, by increasing the inclusions percentage, the differences decrease from 0.7 to 0.4%.

The toughening effect associated with the $t \rightarrow m$ phase transformation was considered, assuming an uniform expansion in all directions and not anisotropic (real case) and neglecting also the tangential components of the deformation. The volume increase of zirconia was taken into account by considering the lower limit of 3% reported by Lange [3]. Therefore, setting the volume of inclusion after transformation equal to that obtained when expansion is due to a uniform increase in temperature ΔT, the following relation is obtained:

$$1.03\frac{4}{3}\pi r_f^3 = \frac{4}{3}\pi r_f^3(1 + \alpha_Z \Delta T)^3 \tag{15}$$

from which ΔT:

$$\Delta T = \frac{\sqrt[3]{1.03} - 1}{\alpha_Z} \tag{16}$$

The effect due to the $t \rightarrow m$ phase transformation could be simply simulated by adding the value of ΔT by the Eq. (16),

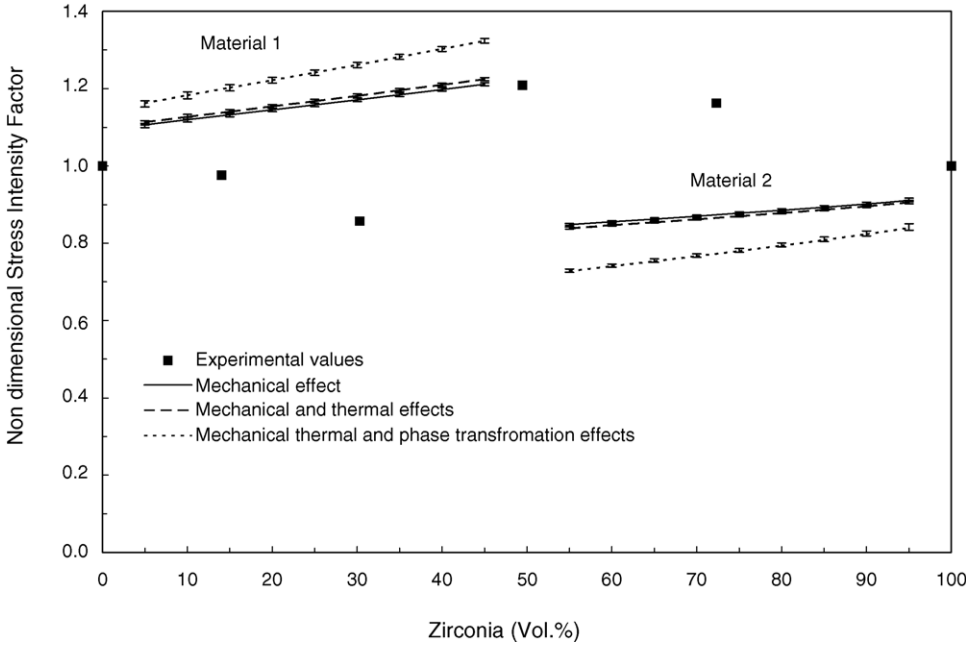

Fig. 5. Dimensionless stress intensity factor, K_I/K_0, as a function of the volume percentage of zirconia, for Materials 1 and 2.

to the field of temperature T of the inclusion. This expansion induces a compressive radial stress that, added to the stress due to the thermal component, leads to a further increase in the stress σ_t acting on the matrix. In comparison with the case in which only the effect of tensile stress is considered, K_I progressively increases from 5 to 9% with the increase of the inclusions percentage. In Fig. 5 are reported also the K_I values concerning a crack of intermediate length. In this case, changing the crack length, the differences decrease from 1 to 0.5% with the increase of the inclusions percentage.

The curve reported in Fig. 5 shows that the increase of the inclusions percentage does not bring any benefit, since K_I tends to increase, and consequently, the fracture resistance decreases. This behaviour is confirmed by the experimental results for the materials 2Z8A and 4Z6A, reported in Table 3. The toughness values were normalised to K_{IC} (4.2 MPa $m^{1/2}$) obtained for the pure material, while the inclusions percentage in weight was converted in volume by the density of alumina and zirconia, reported in Table 2.

The results presented in Table 3, in agreement with the characteristics of the pure materials, indicate a decrease of Young's modulus and Vickers hardness with the increase of the zirconia content. In addition, the increase of the inclusions percentage leads to a progressive increase of the bending strength.

In the analyses carried out on Material 2, both the stresses due to the different thermal expansion coefficient of the materials and the toughening effect associated with the $t \rightarrow m$ phase transformation were taken into consideration. For the latter effect, an uniform expansion in all directions and a volume increase of 3% were supposed. Setting the volume of the matrix after expansion equal to that obtained when the expansion of the matrix is due to an uniform increase in temperature ΔT and neglecting the expansion along the thickness, the following relation can be obtained:

$$1.03\frac{4}{3}\pi(r_m^3 - r_f^3) = \frac{4}{3}\pi(1 + \alpha_Z \Delta T)^3(r_m^3 - r_f^3) \quad (17)$$

From the Eq. (17), the same value of ΔT of the Eq. (16) can be calculated. This value must be added to the field of temperature T of the matrix.

The behaviour of the stress intensity factor obtained from the analysis is reported in Fig. 5. The values of K_I, relative to the crack length $r_m/50$, are normalised to K_0. The upper and lower shifts are relative to crack lengths $2a = r_m/100$ and $2a = r_m/25$, respectively. Unlike for Material 1, the stress intensity factor of Material 2 tends to decrease with an increase of the inclusions percentage, and consequently the bending strength increases. The fracture toughness of materials 8Z2A and 6Z4A, normalised to the value of K_{IC} (4.3 MPa $m^{1/2}$) obtained for Z material, is reported in Fig. 5. To better compare these last experimental results with the values calculated on the basis of the model, the inclusions percentage in weight was converted into the corresponding volume percentage. The experimental results confirm the calculated data. Indeed, as the alumina content increases, also the fracture toughness of the material increases. In this case the values of Young's modulus and Vickers hardness increase, according to the characteristics of the pure materials, Table 3. The increase in the inclusions percentage determines a favourable effect on the bending strength.

4.2. High temperature analysis

The investigation was completed with an analysis at different temperatures of the RVE, Fig. 4. The effects due to the thermal expansion coefficients of the materials and the toughening associated with the $t \rightarrow m$ phase transformation are still considered. In these analyses, both Young's modulus

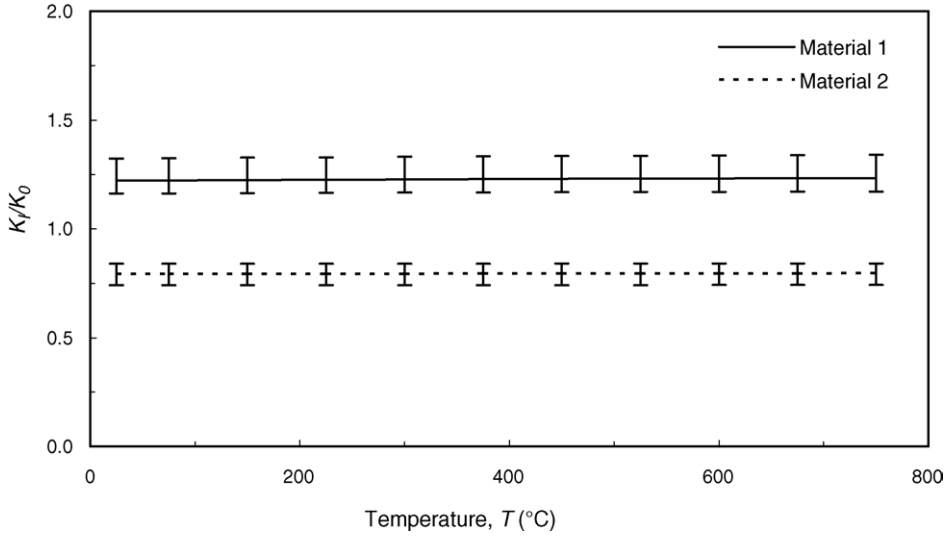

Fig. 6. Dimensionless stress intensity factor, K_I/K_0, as a function temperature, for a 20 vol.% of inclusions and crack length $2a = r_m/50$.

and Poisson's coefficient of alumina and zirconia were assumed to be constant with the temperature.

For Material 1, as the temperature increases, there is, for the same inclusions percentage and crack length, a small increase, 1%, in the stress intensity factor K_I and consequently, a decrease of toughness, Fig. 6. The results are referred to a crack length $r_m/50$, and 20 vol. inclusions percentage. The upper and lower shifts are relative to inclusions percentages of 40 and 5, respectively. These results are in agreement with those reported in [19] where, in the range of temperature here considered, K_{IC} shows a small decrease with the increase of temperature.

The results concerning the Material 2, for a crack length $r_m/50$ and a 20% of inclusions, show a behaviour of K_I practically independent of the temperature. As shown in Fig. 6, the difference between the K_I values corresponding to the bounds of the interval of temperature chosen, is less than 0.3%. In this case the upper and the lower shift are relative to an inclusions percentage of 5 and 40, respectively.

The analyses, for both Materials 1 and 2, did not carried out at temperatures higher than 750 °C, because the monoclinic phase of zirconia is stable only up to a temperature ∼800 °C. The analyses carried out for crack lengths $r_m/25$ and $r_m/100$, greater and smaller than $r_m/50$, respectively, show that the behaviour of the stress intensity factor at different temperatures is similar to that reported in Fig. 6. The change of the crack length is able only to increase or reduce the values of K_I, Fig. 6. In particular, the increase of the crack length determines in the case of the Material 1 a decrease of K_I, while for the Material 2, an increase of K_I. In any case for both the materials, the variation in comparison with the K_I values reported in Fig. 6, is less than 1%.

5. Conclusions

The present investigation deals with a model developed to simulate the effect of toughening in alumina–zirconia composites. The phenomena considered are: (i) the expansion of the inclusions when the zirconia is subjected to a stress able to activate the $t \rightarrow m$ phase transformation, and (ii) the thermal stresses induced during sintering and cooling stage.

The simulation of both phenomena was carried out analysing a simple model based on two concentric spheres and a crack in the matrix near the interface of the inclusion and assigning fields of temperature to the matrix and the inclusions. The results allowed to evaluate the influence on K_I of the temperature, crack length and inclusions percentage.

Even if the model does not take thoroughly into account the toughening mechanism, there is a satisfactory agreement between the numerical results and the experimental data obtained at room temperature. The model, after the experimental validation at high temperature, should be useful to determine the optimum inclusions percentage as a function of the service conditions, also for different kinds of ceramic composites.

References

[1] N. Claussen, Microstructural esign of zirconia toughened ceramics (ZTC), in: Advances in Ceramics, Science and Technology of Zirconia II, American Ceramic Society, Westerville, OH, USA, 1983.

[2] M.H. Bocanegra-Bernal, D. De La Torre, Phase transitions in zirconium dioxide and related materials for high performance engineering ceramics, J. Mater. Sci. 37 (2002) 4947–4971.

[3] F.F. Lange, Transformation toughening Part 4 fabrication, fracture toughness and strength of Al_2O_3–ZrO_2 composites, J. Mater. Sci. 17 (1982) 247–254.

[4] P.M. Kelly, L.R. Francis Rose, The martensitic transformation in ceramics—its role in transformation toughening, Progr. Mater. Sci. 47 (2002) 463–557.

[5] S.J. Glass, D.J. Green, Mechanical properties of infiltrated alumina-Y-TZP composites, J. Am. Ceram. Soc. 79 (1996) 2227–2236.

[6] S. Hori, M. Yoshimura, S. Somiya, R. Kurita, H. Kaji, Mechanical properties of ZrO_2-toughened Al_2O_3 ceramics from CVD powders, J. Mater. Sci. Lett. 4 (1985) 413–416.

[7] J.-F. Li, R. Watanabe, Fracture toughness of Al_2O_3-particle-dispersed Y_2O_3-partially stabilised zirconia, J. Am. Ceram. Soc. 78 (1995) 1079–1082.

[8] D.J. Green, Critical microstructures for microcracking in Al_2O_2–ZrO_2 composites, J. Am. Ceram. Soc. 65 (1982) 610–614.

[9] Q. Ma, V. Pompe, J.D. French, D.R. Clarke, Residual stresses in Al_2O_3–ZrO_2 composites: a test of stochastic stress models, Acta Metall. Mater. 42 (1994) 1673–1681.

[10] E. Merlani, C. Schmid, V. Sergo, Residual stresses in alumina/zirconia composites: effect of cooling rate and grain size, J. Am. Ceram. Soc. 84 (2001) 2962–2968.

[11] S.P. Timoshenko, J.N. Goodier, Theory of Elasticity, McGraw-Hill Book Co, USA, 1970.

[12] S.B. Batdorf, H.L. Heinisch Jr., Weakest link theory reformulated for arbitrary fracture criterion, J. Am. Ceram. 61 (1978) 355–358.

[13] K. Hellen, W.S. Blackburn, The calculation of stress intensity factors for combined tensile and shear loading, Int. J. Fract. 11 (1975) 605–617.

[14] M.F. Kanninen, C.H. Popelar, Advanced Fracture Mechanics, Oxford University Press, USA, 1985.

[15] A. Salomoni, I. Stamenkovic, L. Esposito, A. Tucci, Near-net-shape forming technique for bioceramic components, Ceram. Trans. Bioceram.: Mater. Appl. III 110 (2000) 103–112.

[16] European Standard EN 843-1, Advanced technical ceramics–monolithic ceramics–mechanical properties of monolithic ceramics at room temperature Part 1. Determination of flexural strength, 1995.

[17] G.R. Anstis, P. Chantikul, B.R. Lawn, D.B. Marshall, A critical evaluation of indentation techniques for measuring fracture toughness. I. Direct crack measurements, J. Am. Ceram. Soc. 64 (1981) 533–538.

[18] C. Hillman, Z. Suo, F.F. Lange, Cracking of laminates subjected to biaxial tensile stresses, J. Am. Ceram. Soc. 79 (1996) 2127–2133.

[19] G. Orange, G. Fantozzi, P. Homerin, F. Thevenot, A. Leriche, F. Cambier, Fracture toughness of Al_2O_3–ZrO_2 ceramic composites; effect of microstructure and temperature, in: Proceedings of the Second International Symposium Ceramic Materials and Components for Engines, 1986, pp. 567–574.